JOURNAL OF CATALYSIS 135, 386–399 (1992)

Cobalt-Modified Cu–Zn–Cr Catalysts in the Synthesis of Methanol

G. FORNASARI,* A. D' HUYSSER,† L. MINTCHEV,‡ F. TRIFIRÒ,* AND A. VACCARI*

*Dip. di Chimica Industriale e dei Materiali, Viale Risorgimento 4, 40136 Bologna, Italy; †Lab. Catalyse Hétérogène et Homogène, U.A. 402, 59655 Villeneuve d' Ascq, France; and ‡Institute of Kinetics and Catalysis, Bulgarian Academy of Sciences, 1040 Sofia, Bulgaria

Received April 26, 1991; revised November 12, 1991

The structural modifications and changes in reactivity in the low-temperature synthesis of methanol induced by the presence of small amounts of cobalt in Cu–Zn–Co–Cr catalysts (from 38 : 38 : 0 : 24 to 34 : 38 : 4 : 24, as atomic ratio) were investigated. In all cases homogeneous precursors with a hydrotalcite-type structure were prepared, which upon calcination formed mainly cubic nonstoichiometric spinel-type phases, characterized by an excess of bivalent cations. Also taking into account the presence of cobalt as Co^{3+} ions, as evidenced by XPS, the M^{2+}/M^{3+} ratio was higher than 0.5 (typical of a stoichiometric spinel). Even so, only the cubic spinel-type phase was detected for the sample containing 4.0% of cobalt. During reduction and/or reaction Co^{3+} ions were reduced to Co^{2+} ions, always in octahedral coordination, while the formation of segregated cobalt oxides and/or metallic cobalt was not detected. The presence of small amounts of cobalt led to considerable modification in the surface reactivity of the catalysts. TPR and isothermal reduction tests at 483 K showed both an increase in reducibility of the main copper-containing fraction and the formation of a smaller less reducible fraction. On the other hand, TPD tests showed a considerable increase in the strength of the CO interaction with the surface, which occurred with a decrease in oxidizing capacity of the catalyst surface, as indicated by the values of the CO/CO_2 ratios. The catalytic data showed a change from a low-temperature methanol to a Fischer–Tropsch catalyst, which occurred in two stages: (1) With cobalt content up to 2% a dramatic deactivation was observed without any change in selectivity and (2) at higher cobalt contents an increase in activity was detected, but with a high selectivity in hydrocarbons. This behavior was interpreted as being due to the formation by reduction of the cubic nonstoichiometric spinel-type phase mainly of a highly dispersed metallic copper, not detectable by XRD analysis and probably characterized by low-Miller-index surface planes. The low amounts of cobalt destroyed the catalytic activity by poisoning the oxidizing capacity of the catalyst surface, while further cobalt additions resulted in an increase in the activity with a change in selectivity to hydrocarbons, probably the result of a synergetic effect between the well-dispersed metallic copper and the cobalt-containing cubic spinel-type phase.

INTRODUCTION

Modern industrial catalysts for low-temperature and low-pressure methanol synthesis from syngas ($CO + H_2$) are constituted by mixed oxide systems $CuO–ZnO–M_2O_3$ (M = Al, Cr, V, or Mn) that must be previously activated by reduction procedures (*1–5*). These mixed oxides are usually produced by coprecipitation methods and have been found to be considerably more active than the individual components.

Recently, it has been claimed that the presence of cobalt and potassium in low-temperature methanol catalysts shifts the selectivity toward methanol and higher alcohol mixtures ($C_1–C_6$) (*6–8*). However, it must be pointed out that a strong deactivation of the catalysts for the synthesis of methanol was observed after impregnation with small amounts of cobalt (*9, 10*). It has also been reported that the same effect takes place toward the higher alcohol formation, thus indicating that the reactions leading to both products are related, probably through a common active site or intermediate (*11*)

In a recent paper (*12*) it was proposed that the most active copper surface for CH_3OH

0021-9517/92 $5.00

synthesis may be blocked off by isolated surface cobalt atoms, which, moreover, are capable of accomplishing most of the elementary steps associated with the Fischer–Tropsch reaction of CO with H_2. We have also investigated the catalytic activity of some Co, Cu, Zn, and Cr mixed oxides and the main products obtained were hydrocarbons with typical Schulz–Flory distributions (*13*). Maximum activity was obtained for catalysts containing comparable amounts of copper and cobalt, while the catalytic activity was lower for catalysts with high cobalt contents.

The objective of the research reported in this paper was to study the transition from a methanol catalyst (Cu–Zn–Cr = 38 : 38 : 24, as atomic ratio) to one for the synthesis of high-molecular-weight products, by investigating the effect of increasing amounts of cobalt (0.0–4.0%, as atomic ratio). Differently from the previous works (*9–11*) the cobalt was present starting from the precipitation, thus avoiding possible surface covering or sintering and segregation phenomena, as recently described for the alkalization step by aqueous solutions (*14*). Furthermore, in order to start from homogeneous precursors with a hydrotalcite-type structure, we maintained constant the M^{2+}/M^{3+} and Cu + Co/Zn ratios (*15*, *16*).

METHODS

The precipitates obtained by coprecipitation, i.e., by placing a solution of the nitrates of the elements into a solution of $KHCO_3$ at 333 K, were washed until a minimum potassium content (lower than 0.4%, as K_2O) was obtained, dried at 363 K, and calcined at 623 K for 24 h. The precursor compositions (Table 1) were confirmed by atomic absorption spectroscopy using a Perkin–Elmer 360 spectrophotometer.

XRD powder patterns were obtained with Ni-filtered Cu$K\alpha$ radiation (λ = 0.15418 nm) using a Philips Goniometer equipped with a stepping motor and automated by means of a General Automation 16/240 computer. All the XRD powder patterns were obtained in air. Before XRD analysis, the reduced and/or reacted samples were first passivated with N_2O. Since most of the diffraction patterns showed broad and/or overlapped diffraction lines, both phase composition and crystal size were determined by a profile fitting method, which involved comparing the observed profiles with the computed ones, calculated according to Allegra and Ronca (*17*). The accuracy of this method is better than that of the Debye–Scherrer method, especially when many species are present; however, the precision is similar to that of the Debye–Scherrer method.

A Carlo Erba Sorptomatic 1826 with N_2 adsorption was used to measure the surface area, pore volume, and radius distribution of pores, the latter being calculated by means of Pierce's method (*18*).

XPS spectra were measured on a Leybold–Hereaus LHS 10 spectrometer using nonmonochromatized Al$K\alpha$ radiation. The anode was operated at about −300 W power (13 kV, 23 mA). The samples, pressed on a stainless-steel holder, were mounted on a sample rod that permitted reduction treatments [H_2/N_2 = 10 : 90 (v/v)] up to 673 K in a preparation chamber directly connected to the analysis chamber of the spectrometer. The base pressure during analysis was 1.33×10^{-6} Pa. The spectrometer was operated in fixed analyzer transmission (FAT) with a pass energy of 50 eV. XPS copper $2p_{3/2}$, zinc $2p_{3/2}$, chromium $2p$, cobalt $2p$, oxygen $1s$, and carbon $1s$ were recorded. All binding energies (BE) were referenced to the carbon $1s$ levels (at 285.0 or 289.7 eV) due to graphitic carbon or to carbonate species always observed on the solids (*19*). The reproducibility of the BEs was ±0.2 eV. Semiquantitative surface compositions of different species i and j, with concentrations N_i and N_j, were calculated from their photoelectron peak areas I_{ij} (after correction for instrumental parameters T_{ij}, photoionization cross section σ_{ij}, and electron mean free paths λ_{ij}) using (*20*)

$$\frac{N_i}{N_j} = \frac{I_i}{I_j} \cdot \frac{\sigma_j}{\sigma_i} \cdot \frac{\lambda_j}{\lambda_i} \cdot \frac{T_j}{T_i},$$

with $\lambda_{i,j} \approx KE_{i,j}^{0.75}$ and $T_{i,j} \approx KE_{i,j}^{-1.00}$ (where $KE_{i,j}$ is the kinetic energy of the analyzed photoelectrons). In line peak area computation the background of the spectra was assumed to be linear over the peak width.

The reduction of the calcined samples were investigated in a Perkin-Elmer TGS-2 thermobalance, choosing a weighing sensitivity of 10 μg, a constant temperature (483 K) and using a H_2/He (5 : 95 v/v) gas mixture. Temperature-programmed reduction (TPR) tests were carried out in a homemade laboratory apparatus, using the same reaction gas mixture and a constant rate of temperature increase (5 K min^{-1}) and determining the H_2 consumption by a HWD (hot wire detector). Before introducing the reduction gas mixture, all the samples were pretreated at 623 K in a flow of oxygen-free helium until constant weight was reached.

Temperature-programmed desorption (TPD) experiments were carried out in a home-made laboratory apparatus, previously described (*21*). The desorbed species were analyzed by a HWD and a VG quadrupole mass spectrometer (qms) and the data were processed directly by an Apple II computer. Before the TPD experiments all catalysts were activated in a flow of hydrogen (60 ml h^{-1}) with a constant rate of temperature increase (10 K min^{-1}) up to 670 K, and then held at this temperature for 1 h.

Alternatively some of the samples were reduced in milder conditions using a flow of 5% hydrogen in helium (v/v) (60 ml h^{-1}) and a slower rate of temperature increase (3 K min^{-1}). No differences were observed in the maximum of HWD signals or in TPD peak compositions analyzed by qms.

After cooling at 300 K, the flow was changed from hydrogen to helium and the catalysts saturated with pulses of CH_3OH–He [5 : 95 (v/v)] at 350 K. After 30 min in a pure helium flow at the same temperature, the temperature was increased at a constant rate of 25 K min^{-1} up to 670 K, under a He flow of 60 ml min^{-1}.

The catalytic tests were performed using about 0.3 g of catalyst (0.250–0.425 mm particle size) in a copper fixed-bed tubolar reactor (i.d. 2 mm, length 450 mm), operating at 1.0–2.0 MPa in the 523–623 K range, with GHSV of 2,000–16,500 h^{-1} and a $H_2/CO/CO_2$ = 65/32/3 (v/v) gas mixture. The reaction products were analyzed in-line by a Carlo Erba 4300 gas chromatograph equipped with FID (flame ionization detector) and two columns (3.2 mm × 2.0 m) fitted with Poropack QS. After condensation of the other compounds at 253 K, the gases were analyzed with a Carlo Erba 4300 gas chromatograph equipped with HWD and two columns (3.2 mm × 2.0 m) fitted with Carbosieve S. The chromatographic data were collected and processed by a Perkin-Elmer Sigma 15 data station. Before reaction, the catalysts were activated by reduction, using hydrogen diluted in nitrogen, and progressively increasing the hydrogen concentration and the temperature (*8*). After reaction, the catalysts were cooled at room temperature under a flow of oxygen-free helium, titrated with N_2O (see below) and extracted from the reactor.

The surface area of the copper was determined *in situ* after reaction and/or further reduction by the N_2O pulse technique (*22–24*). Before measuring the surface area, the samples were cooled at room temperature under a flow of oxygen-free helium. Preliminary tests on Cr_2O_3, Zn/Cr, and Co/Cr samples did not reveal decomposition or adsorption of N_2O.

RESULTS AND DISCUSSION

XRD Powder Analysis

Reported in Table 1 are the catalyst compositions and the phases identified by XRD analysis after drying, calcination, and reaction. Reported in Fig. 1, as an example, are the XRD powder patterns of two samples after the different steps. All dried precursors showed the presence of only hydrotalcite-type phases with small crystal size and very

TABLE 1

Nature of the Phases Identified after the Different Steps by XRD Analysis

Cu : Zn : Co : Cr (atomic ratio)	Notation	After drying at 363 K for 24 h	After calcination at 623 K for 24 h	After reaction and reoxidation
38.0 : 38.0 : 0.0 : 24.0	Co-0.0	HT	Spin.; ZnO; CuO	Spin.; ZnO; CuO
37.8 : 38.0 : 0.2 : 24.0	Co-0.2	HT	Spin.; ZnO; CuO	Spin.; ZnO; CuO
37.0 : 38.0 : 1.0 : 24.0	Co-1.0	HT	Spin.; ZnO; CuO[a]	Spin.; ZnO; CuO
36.0 : 38.0 : 2.0 : 24.0	Co-2.0	HT	Spin.; ZnO	Spin.; ZnO; CuO
34.0 : 38.0 : 4.0 : 24.0	Co-4.0	HT	Spin.	Spin.; CuO

Note. HT, hydrotalcite-type phase. Spin., cubic spinel-type phase.
[a] Very small amounts.

similar values of the crystallographic parameters a and c. Therefore, the presence of cobalt did not influence the structure of the precursors, which were homogeneous in all cases.

After calcination, all catalysts showed a microcrystalline cubic spinel-type phase as the main phase, together with some amounts of ZnO and CuO (Table 1 and Fig. 1). Formation of cobalt oxides was never observed, although it is not possible to exclude their presence in very small amounts. The decrease in the oxide segregation with increasing cobalt content should be emphasized. In fact, for catalyst Co-4.0, only a cubic spinel-type phase was identified. The crystallographic parameters of cubic spinel-type phases in the samples calcined or extracted from the reactor after the catalytic tests are reported in Table 2.

By hypothesizing the total oxidation of

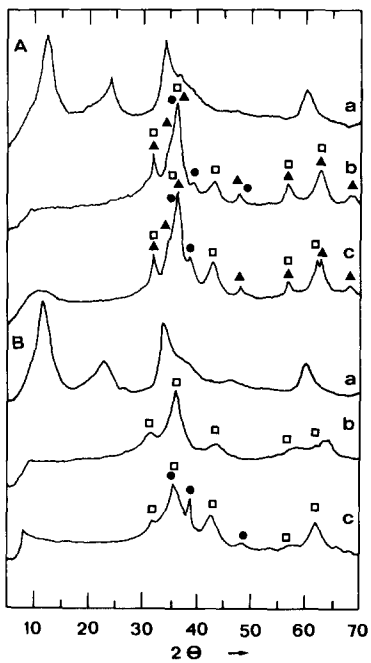

FIG. 1. XRD powder patterns of the samples (A) Co-1.0 and (B) Co-4.0 after (a) precipitation, (b) calcination, and (c) reaction. (▲) ZnO; (●) CuO; (□) spinel-type phase.

TABLE 2

Crystallographic Parameters of the Spinel-type Phases after Calcination for 24 h at 623 K and after Reaction

Sample	Lattice parameter a (nm)		Crystal size (nm)	
	After calcination	After reaction[a]	After calcination	After reaction[a]
Co-0.0	0.8416	n.d.	4.0	4.5
Co-0.2	0.8438	0.8450	4.0	4.0
Co-1.0	0.8421	0.8458	4.0	4.0
Co-2.0	0.8421	0.8451	4.5	4.5
Co-4.0	0.8475	0.8501	2.5	3.0

Note. $ZnCr_2O_4$ = 0.8327 nm (ASTM 22–1107); $CoCr_2O_4$ = 0.8330 nm (ASTM 22–1084); Co_2CrO_4 = 0.8170 nm (ASTM 24–326); Co_3O_4 = 0.8084 (ASTM 9–418); CoO = 0.8520 (ASTM 9–402).
[a] After reaction and following reoxidation. After a further reduction/reoxidation step, all samples showed the lattice parameter a and crystal size similar to those determined after reaction and reoxidation.

Co^{2+} ions to Co^{3+} ions during the calcination and the presence in the calcined samples of a simple phase mixture of stoichiometric $M^{2+}M_2^{3+}O_4^{2-}$ spinel and $M^{2+}O^{2-}$ oxide phases (where M^{2+} = Cu^{2+}, Zn^{2+} and M^{3+} = Cr^{3+}, Co^{3+} ions) the weight percentage of the oxide phases should range from ~65 to 58% for the Co-0.0 and Co-4.0 samples, respectively.

On the contrary, for all calcined samples the XRD analysis showed the cubic spinel-type phase as the main phase, with the oxide phases present in lower amounts or fully absent, as for the Co-4.0 sample. Therefore, there is a large fraction of the calculated oxides, which escapes the XRD detection. In analogy to that previously reported for similar systems (*13, 25–28*), the presence of an excess of bivalent cations inside the cubic spinel-type phases formed by calcination may be hypothesized. These phases may be described by the general formula $M_x^{2+}M_{2/3(1-x)}^{3+}O^{2-}$ or the equivalent $M_{1+y}^{2+}M_{2-2/3y}^{3+}O_4^{2-}$ (with $y = 4x-1$). The higher the value of x the more M^{2+} ions are located in octahedral sites, randomly substituted by Cr^{3+} and Co^{3+} ions, and, consequently, more tetrahedral sites are left vacant.

After reaction and following reoxidation, the cubic spinel-type phase was again present as the main phase in all samples, with a partial evolution for the cobalt-rich samples toward a rock salt-type structure related to the reduction of the Co^{3+} ions to Co^{2+} ions and their permanence in the octahedral sites due to the low ionic mobility in our experimental conditions. Formation of metallic cobalt and/or cobalt oxides was not observed, although their presence has been reported for other copper–cobalt-based catalysts (*7, 9*). It is not possible however to exclude their presence in very small amounts that are not detected by XRD analysis. On the other hand, these data are in agreement with the reducibility at high temperature of the cobalt oxides, reported by Arnoldy and Moulijn (*29*).

In these samples, CuO will small crystal size was detected also for the cobalt-rich samples, in which it was absent after calcination, showing that it may partially come from the reoxidation of metallic copper segregated from the spinel-type phase. On the other hand, the ZnO phase did not show significant changes. However, it is worth noting that also in these samples a fraction of the oxide phases escapes the XRD detection.

TABLE 3

BET Surface Area and Pore Volume of the Samples Calcined for 24 h at 623 K and Copper Surface Area of the Catalysts after Reduction and Reaction

Sample	Surface area (m^2g^{-1})	Pore volume (cm^3 g^{-1})	Copper surface area (m^2 g^{-1} Cu)		
			After reduction	After reaction	After reduct.[a]
Co-0.0	96	0.959	45	20	42
Co-0.2	93	1.212	43	36	45
Co-1.0	94	0.853	43	3	35
Co-2.0	88	0.912	36	<1	30
Co-4.0	149	0.542	25	<1	20

[a] Further reduction *in situ* after the catalytic tests.

Surface Area and Pore Volume Determinations

The values of surface area and pore volume determined by N_2 adsorption are reported in Table 3. The same table also shows the values of the metallic copper surface area determined after reduction, catalytic tests, and further reduction.

The synthesis of hydrotalcite-type precursors favored the formation by calcination of samples with high surface areas. The very high surface area of the Co-4.0 sample, for which only the presence of a spinel-type phase was detected, should be noted. This sample also had lower value pore volume and a lower average pore radius with a narrow pore-size distribution.

After reaction, the Co-0.0 and Co-0.2 catalysts showed decreases in metallic copper surface area similar to those previously re-

TABLE 4

XPS Surface Compositions of the Catalysts in the Different Steps

Sample	Cu/Zn atomic ratio			Cr/Zn atomic ratio			Co/Zn atomic ratio		
	Nominal value	Value after calcination	Value after reaction[a]	Nominal value	Value after calcination	Value after reaction[a]	Nominal value	Value after calcination	Value after reaction[a]
Co-0.0	1.00	0.92	0.67	0.63	0.75	0.76	0.00	n.d.	n.d.
Co-0.2	0.99	0.95	0.92	0.63	0.79	0.68	0.01	n.d.	n.d.
Co-1.0	0.97	1.01	0.82	0.63	0.79	0.75	0.03	0.02	0.02
Co-2.0	0.95	0.92	0.89	0.63	0.80	0.71	0.05	0.03	0.03
Co-4.0	0.89	0.82	0.48	0.63	0.79	0.75	0.11	0.14	0.23

[a] After reaction and following reoxidation.

ported and attributed to partial oxidation of the surface (*30*), while for the other samples the surface area became negligible. However, upon further reduction, all spent catalysts had practically the same values of the copper surface area as after the first reduction step. Therefore, the considerable decrease observed for the cobalt-rich catalysts must be attributed to a reversible poisoning of the surface, instead of sintering phenomena.

On the other hand, also for the spinel-type phase no sintering phenomena took place during the catalytic tests, as evidenced by the similar values of crystal size for the samples calcined and discharged from the reactor (Table 2).

XPS Analysis

The nominal compositions and those determined in the calcined samples and in the samples extracted from the reactor after the catalytic tests are reported in Table 4. No significant differences from the nominal compositions were observed after calcination, showing that little oxide segregations occurred. This may be attributed to the hydrotalcite-type structure of the precursors, in which all elements are homogeneously distributed in the brucite-like layers, and no surface enrichment takes place during their decomposition.

After reaction and reoxidation, the chromium and zinc surface contents did not change appreciably in comparison with those for the samples after calcination, showing that the two elements are strongly interacting very probably in a cubic spinel-type phase. On the contrary, the change in the copper and cobalt surface contents for the Co-0.0 and Co-4.0 catalysts in comparison with those of the calcined samples should be noted.

In order to better understand the behavior of the copper and cobalt species and particularly to specify their valence state in these two compounds, we focused particular attention on the Cu $2p_{3/2}$, Cu L_3 $M_{4.5}$ $M_{4.5}$, and Co $2p$ XPS regions of the samples after calcination, reaction/reoxidation, and further reduction *in situ* by H_2 at 523 K (Fig. 2). This last treatment was performed in order to evidence if the Cu^{2+} ions derived from the reoxidation of the metallic copper after the catalytic tests or were stabilized in the

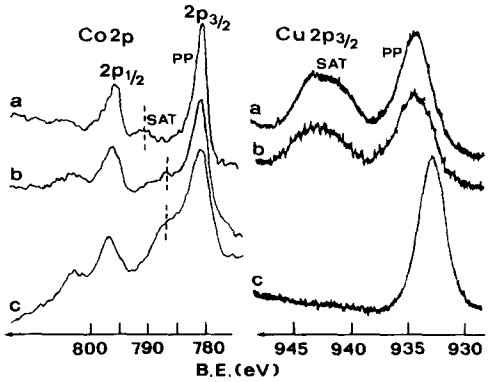

FIG. 2. Co $2p$ and Cu $2p_{3/2}$ XPS lines for the Co-4.0 sample after different treatments: (a) calcination, (b) reaction, and (c) further reduction.

cubic spinel-type phase. Drastic changes were observed in the line shape as a function of the treatment. Identification of the photoexcited chemical species were obtained through some of their significant spectroscopic features: shape of the peaks, presence of more or less intense satellite (SAT) structures, binding or kinetic energies of the different components of the lines.

The main results obtained are reported in Table 5, together with the line assignments. It appeared that:

(1) In the calcined samples and in the samples extracted from the reactor after the catalytic tests, copper was in the Cu^{2+} state. This is shown by the SAT structures of the lines, which are fingerprints of Cu^{2+} (*31*). On the other hand, the further reduction *in situ* by H_2 gave rise to the complete reduction to metallic copper [absence of SAT structures and Auger parameter of 1851.4 ± 0.3 eV typical of metallic copper, instead of 1849.3 ± 0.3 eV, as in the case of Cu^+ ions (*32, 33*)].

(2) After calcination, cobalt was present as octahedral Co^{3+}, as indicated by a low-intensity SAT structure at about 9.4 eV from the $2p_{3/2}$ main peak (*34*).

(3) The catalytic tests reduced Co^{3+} ions to Co^{2+} ions, which remained localized into the octahedral sites of the cubic spinel-type matrix. This is mainly proved by the typical high-intensity SAT structures at about 6 eV from the 2*p* principal lines, added to the fact that the binding energies of these peaks are different from those of octahedral Co^{2+} in the simple oxide CoO (*35*) and tetrahedral Co^{2+} in mixed oxide spinels, like $CoCr_2O_4$ (*34*). No significant changes were observed after further reduction *in situ* by H_2. In particular, metallic cobalt also was not detected after this step.

Taking into account these results, which are consistent with the XRD analysis, the changes observed for the Cu/Zn and Co/Zn surface ratios can be explained (1) for the Co-0.0 sample, by a partial segregation of copper, thus evidencing as an indirect consequence a stabilization effect of cobalt in the cubic spinel-type matrix of the catalysts with lowest cobalt contents and (2) for the Co-4.0 sample, by a cobalt enrichment of the surface, probably due to the migration of octahedral Co^{2+} ions and an exchange with Cu^{2+} ions within the same coordination (ionic radii 0.69 and 0.74 Å, respectively). Nevertheless, the considerable copper content decrease observed for this sample is only partially balanced by a cobalt content increase (Cu + Co/Zn = 0.71 after reaction and reoxidation against 0.93 after calcination) so that segregation of small copper particles must go with the migration of Co^{2+} ions during catalytic tests.

Study of the Reduction Step

The TPR profiles of the different calcined samples are shown in Fig. 3, in which for sake of comparison the curve of the sample Co-19.0 (Cu : Zn : Co : Cr = 19 : 38 : 19 : 24) is also reported. The TPR profiles showed a progressive deplacement from 500 to 470 K of the reduction temperature of the Cu^{2+} ions with increasing cobalt content. Furthermore, for the cobalt-rich samples, an additional reduction peak at 675–700 K was also observed, attributable to the reduction of Co^{2+} ions with the formation of metallic particles (*29, 36–39*).

Further information was obtained by carrying out isothermal reduction at 483 K, i.e., at a temperature to which only CuO is reduced [cobalt oxides are reduced at about 650 K (*29, 36–39*)]. On the other hand it is known that copper activates the reduction of cobalt (*40*). It must be emphasized however that only a very low percentage of cobalt oxides (from 0 to 5%) was reduced up to 513–523 K (*7*). Therefore, since we used a lower reduction temperature in our experiments, it can be hypothesized that the percentage of cobalt that may have been reduced was almost negligible. Furthermore in our catalysts no evidence of metallic cobalt by XRD or XPS analyses was found, even though it is not possible to exclude its presence in very small amounts.

Reported in Fig. 4 are the curves of the

TABLE 5

Main Spectral Features and Chemical States of Copper and Cobalt in Co-0.0 and Co-4.0 Catalysts

	Copper				Cobalt		
	E_B	E_K	α'	Assignment	E_B	ΔE	Assignment
Co-0.0[a]	934.5			Cu^{2+}			
Co-0.0[b]	934.4			Cu^{2+}			
Co-0.0[c]	933.3	918.2	1851.5	Cu^0			
Co-4.0[a]	934.6			Cu^{2+}	780.9	9.4	Co^{3+} octahedral
Co-4.0[b]	934.6			Cu^{2+}	781.0	≅6	Co^{2+} octahedral
Co-4.0[c]	933.0	918.4	1851.4	Cu^0	781.0	≅6	Co^{2+} octahedral

Note. E_B, Binding energy of the principal peak (PP) of the $2p_{3/2}$ level. E_K, Kinetic energy of the $CuL_3M_{4,5}M_{4,5}$ Auger transition. α', Cu Auger parameter: sum of the Cu $2p_{3/2}$ binding energy and the $CuL_3M_{4,5}M_{4,5}$ Auger transition kinetic energy. ΔE, Separation between the satellite structure (SAT) and the principal peak for the Co $2p_{3/2}$ level.

[a] After calcination.

[b] After reaction and reoxidation.

[c] After a further reduction *in situ*.

isothermal reductions, obtained by plotting the fraction of CuO reduced as a function of time (*41–43*), calculated on the basis of weight loss due to the reaction $CuO + H_2 \rightarrow Cu + H_2O$. The maximum value was 1.0, confirming the hypothesis that only CuO was reduced and no adsorption of water took place.

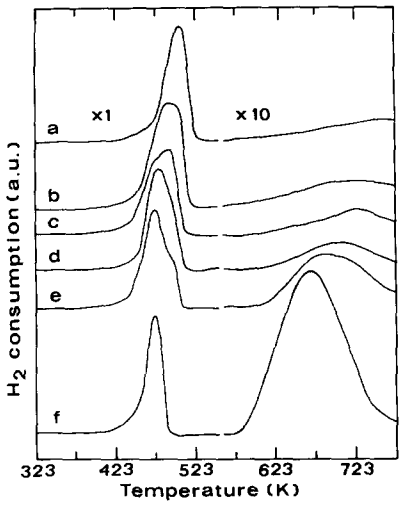

FIG. 3. TPR profiles of the different catalysts calcined at 623 K for 24 h: (a) Co-0.0; (b) Co-0.2; (c) Co-1.0; (d) Co-2.0; (e) Co-4.0. For the sake of comparison the TPR behavior of a sample containing 19% cobalt is also reported (f).

The catalysts showed different behaviors as a function of the cobalt content. In the sample Co-0.0, the copper was completely reduced after 90 min, while in catalyst Co-4.0 after 150 min only 80% of copper was reduced. However, the increase in the rate of reduction (evidenced by an increase in the slope) in the first part of the curve of this last sample should be noted. Therefore, the presence of cobalt gave rise to two different effects:

(1) An increase in reducibility of the main fraction of copper.

(2) Formation, in smaller amounts, of copper-containing species, which are characterized under these conditions by a lower or partial reducibility.

Temperature-Programmed Desorption Tests

Reported in Fig. 5 are the methanol-TPD profiles as determined by HWD. The cobalt-free catalyst showed the presence of two desorption peaks at about 413 and 473 K. When cobalt was present an additional peak at 543 K was also detected, which increased in intensity with increasing cobalt content

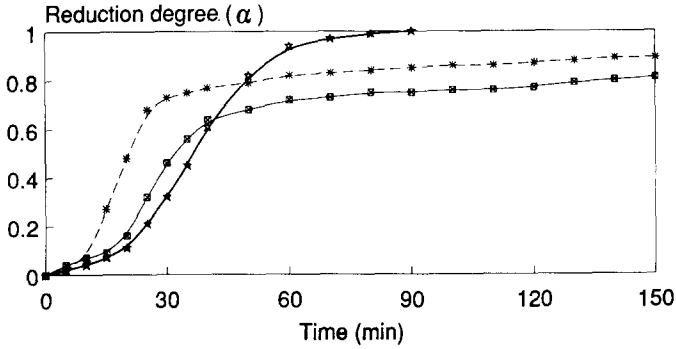

FIG. 4. Isothermal reduction curves at 483 K for the samples (☆) Co-0.0; (*) Co-2.0; and (☒) Co-4-0.

in the catalysts. Furthermore, the presence of 0.2% cobalt was enough to considerably decrease the total amount of desorbed species. A further increase in cobalt content caused the amount of desorbed species to increase again, which, however, up to 4.0% cobalt, remained less than that for the cobalt-free catalysts. On the basis of the qms analyses of the nature and relative amounts of desorbed species it was possible to determine that the peak at 413 K consisted mainly of physically adsorbed methanol. On the other hand, the peak at 473 K consisted of H_2, CO, CO_2, and H_2O, with very small amounts of other compounds.

The increase in cobalt content gave rise to a shift in the desorption temperature of a large fraction of CO, which was the main component of the desorption peak at 543 K, together with a small amount of hydrocarbons.

The values of the ratio between the amounts of desorbed CO and CO_2 are reported in Table 6. With increasing cobalt content this ratio increases from about 1.0 (cobalt-free catalyst) up to 4.0 (Co-4.0 sample). These values show that the first additions of cobalt destroyed the decomposition of methanol via formates to H_2 and CO_2 (*21*).

The addition of cobalt to low-temperature methanol catalysts, therefore, results in the formation of strongly adsorbed species (mainly CO) and also considerably decreases the oxidizing properties of the cata-

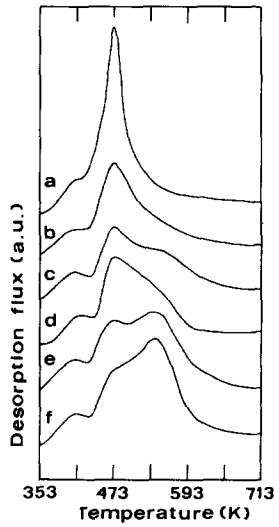

FIG. 5. Total TPD peaks, as determined by HWD, for the different catalysts: (a) Co-0.0; (b) Co-0.2; (c) Co-1.0; (d) Co-2.0; (e) Co-4.0. For the sake of comparison, the curve for a sample containing 19% cobalt is also reported (f).

TABLE 6

CO/CO_2 Ratio (a.u) in the Temperature-Programmed Desorption Tests of Methanol

Sample:	Co-0.0	Co-0.2	Co-1.0	Co-2.0	Co-4.0	Co-19.0
	0.9	1.3	2.0	2.8	4.0	4.0

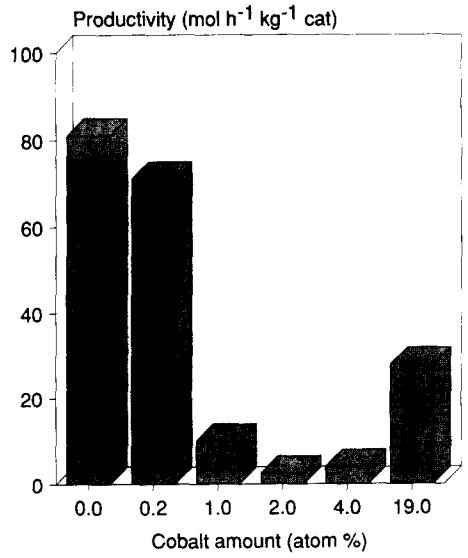

FIG. 6. Total productivity in hydrogenated compounds (methanol and hydrocarbons) as a function of cobalt content (T = 533 K; P = 1.2 MPa; $GHSV$ = 15,000 h^{-1}). For the sake of comparison the datum for a catalyst with a high cobalt content is also reported (*13*).

lyst surface. It is worth noting that 0.2% cobalt was enough to modify the desorption behavior of the catalyst.

Catalytic Activity

The addition of small amounts of cobalt gave rise to a strong deactivating effect (Fig. 6), with a minimum of activity for the Co-2.0 catalyst (about 50 times lower than the activity of the cobalt-free catalyst Co-0.0). Beyond this value, the activity increased again with increasing cobalt content, but with a dramatic change in selectivity toward hydrocarbon formation.

It must be pointed out that the deactivation observed cannot be related to physical factors, since the differences in BET surface area after calcination or copper surface area after reduction (Table 3) do not account for the strong decrease in catalytic activity. The observed decrease in catalytic activity may be attributed to specific cobalt–copper interactions involving the formation of mixed phases, stable in the reaction conditions and responsible for a reversible poisoning of the surface (Table 3). The formation of mixed phases with a homogeneous distribution of the element has already been reported in the literature for low-temperature methanol synthesis catalysts (*44*).

Reported in Fig. 7 are the selectivities in methanol, paraffins, and olefins under reaction conditions typical of low-temperature methanol synthesis. Catalyst Co-0.0 was highly selective in methanol, while catalyst Co-4.0 showed almost comparable selectivities in methanol and hydrocarbons (paraffins + olefins), notwithstanding its low cobalt content.

On the other hand, the reaction conditions of Fig. 8 are those used in Fischer–Tropsch synthesis (i.e., higher temperature and lower GHSV than those used for methanol synthesis). The selectivity changed completely as the amount of cobalt increased from 0.0 to 4.0%. The Co-0.0 sample was still selective in methanol with only traces of methane formation. On the contrary, the Co-4.0 sample showed the typical behavior of a Fischer–Tropsch catalyst, giving rise only to hydrocarbons and only traces of oxygenate compounds. It must be pointed out

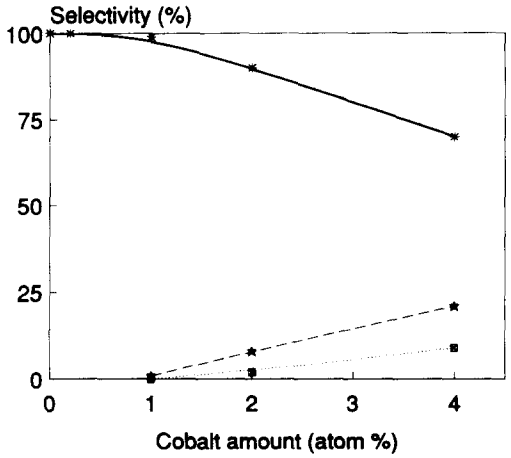

FIG. 7. Lumped selectivity (on C atom basis) as a function of cobalt content. Reaction conditions: T = 533 K; P = 1.2 MPa; $GHSV$ = 15,000 h^{-1}. (*) Methanol; (☆) paraffins; (☒) olefins.

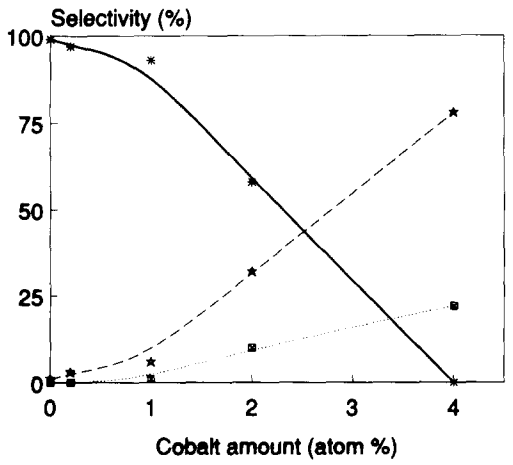

FIG. 8. Lumped selectivity (on C atom basis) as a function of cobalt content. Reaction conditions: T = 563 K; P = 1.2 MPa; $GHSV$ = 3600 h^{-1}. (*) Methanol; (☆) paraffins; (☒) olefins.

that the strong change in selectivity occurred for cobalt contents higher than 1.0%. Beyond this value the formation of paraffins increased considerably and the increase in the amount of olefins formed was linear with cobalt percentage.

The product distributions obtained with the different catalysts are illustrated in Fig. 9. The catalysts with cobalt contents up to 1.0% exhibited, besides methanol, only methane as a byproduct, while, with increasing cobalt content, homologation products began to form and methanol disappeared. On the other hand, the catalyst Co-4.0 produced a range of hydrocarbons varying in carbon number from C_1 to C_7. The hydrocarbons showed a Schulz–Flory-type distribution (*4, 45*), with the amounts of C_1 and C_2 hydrocarbons lower than that to be expected based on a straight line relationship. This is only partially in agreement with data reported for iron- and cobalt-based Fischer–Tropsch catalysts (*46–48*), where the CH_4 selectivity is clearly higher than expected, while with our catalysts methanation is reduced considerably.

CONCLUSIONS

For all samples we started from homogeneous precursors with a hydrotalcite-type structure and characterized by M^{2+}/M^{3+} = 3.0, i.e., much higher than the value required for the formation of a stoichiometric spinel (M^{2+}/M^{3+} = 0.5). Therefore, after calcination consistent amounts of ZnO and CuO should be present together with the spinel phase. On the contrary, we observed only small oxide segregations, the amount of which decreased with increasing cobalt content. In the Co-4.0 sample only a cubic spinel-type phase was detected, with small crystal size and high surface area. Therefore, the formation of cubic nonstoichiometric spinel-type phases characterized by an excess of bivalent cations may be hypothesized, also taking into account the oxidation of the Co^{2+} ions to Co^{3+} ions, as shown by XPS analysis, and the amounts of oxides segregated. This hypothesis is also supported by XPS analysis that shows a homogeneous distribution of the cations, with surface ratios similar to the nominal bulk values.

The catalytic tests increased the segregation of the oxides and CuO was detected in

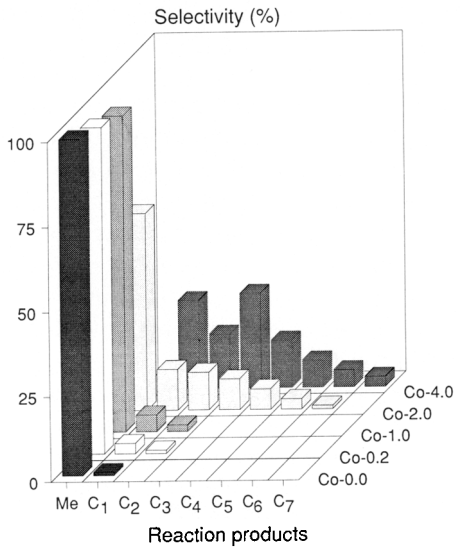

FIG. 9. Selectivity (on C atom basis) in the different compounds for the catalysts with different cobalt contents [Me = methanol; C_1–C_7 = Hydrocarbons (paraffins + olefins)]. Reaction conditions: T = 563 K; P = 1.2 MPa; $GHSV$ = 3600 h^{-1}.

all samples. However, the presence of cobalt oxides and/or metallic cobalt was never observed by either XRD and XPS analyses. On the other hand, the XPS analysis of the samples reduced *in situ* by H_2 showed the presence only of metallic copper. Therefore, it may be hypothesized that in the reaction conditions the copper was present as metallic copper [partially oxidized at the surface (*30, 49*)], which was reoxidized to CuO by treatment at room temperature with N_2O.

For all samples, the zinc and chromium contents in the catalyst surface did not change during reaction, showing that the two elements formed stable cubic spinel-type phases. For the Co-4.0 sample, a decrease in copper and a corresponding enrichment in cobalt content was detected, attributable to both partial segregation of copper and migration of octahedral Co^{2+} ions toward the surface. However, the Co^{2+} ions maintained octahedral coordination, unusual for spinel chromites, as evidenced by both XPS and XRD analysis. This fact may be interpreted taking into account that the cobalt was present in the calcined samples as octahedral Co^{3+} ions (randomly substituted for the Cr^{3+} ions) which by reduction gave rise to Co^{2+} ions with the same symmetry, due to the low temperature of both reduction and reaction, which did not allow structural rearrangement.

The presence of small amounts of cobalt resulted in a considerable modification in the surface reactivity of the catalysts. TPR tests showed a progressive lowering of the reduction temperature of the main fraction of copper as cobalt content increased, with a behavior similar to that of free CuO (*37, 50*). On the other hand, the isothermal tests at 483 K showed the formation of another copper-containing fraction (less than about 20% for the Co-4.0 sample) with a slower rate of reduction, probably a result of a specific interaction with the cobalt ions present in the cubic spinel-type phases.

Based on the catalytic data, the change from a low-temperature methanol to a Fischer–Tropsch catalyst occurs in two stages:

(1) With cobalt contents up to 2.0%, dramatic deactivation was observed without a change in selectivity.

(2) At higher cobalt contents, an increase in activity was detected, but with the formation of hydrocarbons.

On the other hand, the TPD tests showed a considerable increase in the CO interaction with the catalyst surface related to the presence of cobalt, which occurred with a change in the CO/CO_2 ratio from about 1 to 4. The strongest interaction of CO with the surface was also responsible for the dramatic decrease in the copper surface area after reaction, not attributable to sintering phenomena, since when these catalysts were reduced again, values similar to those observed after the first reduction were obtained. Therefore, the addition of small amounts of cobalt to catalysts for the low-temperature synthesis of methanol strongly reduced the oxidizing capacity of the surface, increasing at the same time the strength of CO interaction with the surface.

In a recent paper (*12*) it was proposed that only a small fraction of the copper surface area is active for methanol synthesis and that this fraction is blocked when cobalt is added to the catalysts. However, the same authors claimed that CO and H_2 adsorption took place on the main fraction of copper, which expose a large fraction of high-Miller-index surface planes (*51, 52*).

On the basis of the data reported here, we may hypothesize that the first addition of cobalt poisons the oxidizing capacity (*30, 49, 53*) of a well-dispersed and most active fraction of copper, not detectable by XRD analysis, coming from the reduction of the cubic spinel-type phase and probably characterized by a large fraction of low-Miller-index crystal planes (*54, 55*). On the other hand, it is well known that small amounts of a doping element may strongly modify the physicochemical and catalytic properties of metallic copper (*56, 57*).

By increasing the amount of cobalt, new sites are formed capable of strongly adsorbing the CO and dissociating the C–O bond. Under these conditions the activity increased again, but with synthesis of hydrocarbons. This increase in activity may be attributed to a specific interaction between the well-dispersed metallic copper formed in reducing conditions and the cubic spinel-type phase containing Co^{2+} ions, in agreement with that previously reported (*13*).

ACKNOWLEDGMENTS

Financial support from the Italian Ministry for University and Scientific and Technological Research (MURST, Rome) is gratefully acknowledged. We thank Dr. G. Del Piero (ENIRICERCHE, S. Donato Milanese) for valuable discussions and critical suggestions.

REFERENCES

1. Natta, G., *in* "Catalysis" (P. Emmet, Ed.), Vol. 3, Chap. 8. Reinhold, New York, 1953.
2. Kung, H. H., *Catal. Rev.-Sci. Eng.* **23,** 235 (1980).
3. Klier, K., *in* "Advances in Catalysis" (D. D. Eley, H. Pines, and P. B. Weisz, Eds.), Vol. 31, p. 243. Academic Press, New York, 1982.
4. Henrici-Olivé, G., and Olivé, S., "The Chemistry of the Catalyzed Hydrogenation of Carbon Monoxide," Chap. 8. Springer-Verlag, Berlin, 1984.
5. Chinchen, G. C., Denny, P. J., Jennings, J. R., Spencer, M. S., and Waugh, K. C., *Appl. Catal.* **36,** 1 (1988).
6. Sugier, A., and Freund, E., French Patent 2,369,234 (1976).
7. Courty, P., Durand, E., Freund, E., and Sugier, A., *J. Mol. Catal.* **17,** 241 (1982).
8. Courty, P., Durand, E., Sugier, A., and Freund, E., UK Patent 2,118,061A (1983).
9. Lin, F. N., and Pennella, F., *in* "Catalytic Conversion of Synthesis Gas and Alcohols to Chemicals" (R. G. Herman, Ed.), p. 53. Plenum Press, New York, 1984.
10. Elliott, D. J., and Pennella, F., *J. Catal.* **102,** 464 (1986).
11. Elliott, D. J., *J. Catal.* **111,** 445 (1988).
12. Cao, R., Pan, W. X., and Griffin, G. L., *Langmuir* **4,** 1108 (1988).
13. Fornasari, G., Gusi, S., Trifirò, F., and Vaccari, A., *Ind. Eng. Chem. Res.* **26,** 150 (1987).
14. Szymanski, R., Travers, C, Chaumette, P., Courty, P., and Durand, D., *in* "Preparation of Catalysts IV" (B. Delmon, P. Grange, P. A. Jacobs, and G. Poncelet, Eds.), p. 739. Elsevier, Amsterdam, 1987.
15. Gherardi, P., Ruggeri, O., Trifirò, F., Vaccari, A., Del Piero, G., Manara, B., and Notari, B., *in* "Preparation of Catalysts III" (G. Poncelet, P. Grange, and P. A. Jacobs, Eds.), p. 723. Elsevier, Amsterdam, 1983.
16. Gusi, S., Pizzoli, F., Trifirò, F., Vaccari, A., and Del Piero, G., *in* "Preparation of Catalysts IV" (B. Delmon, P. Grange, P. A. Jacobs, and G. Poncelet, Eds.), p. 753 Elsevier, Amsterdam, 1987.
17. Allegra, G., and Ronca, G., *Acta Crystallogr. Sect. A* **34,** 1006 (1978).
18. Pierce, C., *J. Phys. Chem.* **57,** 149 (1953).
19. Johansson, G., Hedman, J., Berndtsson, A., Klasson, M., and Nilsson, B., *J. Electron Spectrosc. Relat. Phenom.* **2,** 295 (1973).
20. Carter, W. J., Schweitzer, G. K., and Carlson, T. A., *J. Electron Spectrosc. Relat. Phenom.* **5,** 827 (1974).
21. Riva, A., Trifirò, F., Vaccari, A., Mintchev L., and Busca, G., *J. Chem. Soc. Faraday Trans. 1* **84,** 1423 (1988).
22. Osinga, T. J., Linsen, B. G., and Van Beet, W. P., *J. Catal.* **7,** 277 (1967).
23. Dvorak, P., and Pasek, J., *J. Catal.* **18,** 108 (1970).
24. Evans, J. W., Wainwright, M. S., Bridgewater, A. J., and Young, D. J., *Appl. Catal.* **7,** 75 (1983).
25. Del Piero, G., Trifirò, F., and Vaccari, A., *J. Chem. Soc. Chem. Commun.,* 656 (1984).
26. Del Piero, G., Di Conca, M., Trifirò, F., and Vaccari, A., *in* "Reactivity of Solids" (P. Barret and L. C. Dufour, Eds.), p. 1029. Elsevier, Amsterdam, 1985.
27. Bertoldi, M., Fubini, B., Giamello, E., Busca, G., Trifirò, F., and Vaccari, A., *J. Chem. Soc. Faraday Trans. 1* **84,** 1405 (1988).
28. Busca, G., Trifirò, F., and Vaccari, A., *Langmuir* **6,** 1440 (1990).
29. Arnoldy, P., and Moulijn, J. A., *J. Catal.* **93,** 38 (1985).
30. Gusi, S., Trifirò, F., Vaccari, A., and Del Piero, G., *J. Catal.* **94,** 120 (1985).
31. Frost, D. C., Ishitani, A., and McDowell, C. A., *Mol. Phys.* **24,** 861 (1972).
32. Wagner, C. D., and Joshi, A., *J. Electron Spectrosc. Relat. Phenom.* **47,** 283 (1988).
33. Wagner, C. D., *in* "Practical Surface Analysis by Auger and X-ray Photoelectron Spectroscopy" (D. Briggs and M. P. Seah, Eds.), p. 477. Wiley, New York, 1983.
34. Lenglet, M., D'Huysser, A., and Dürr, J., *Ann. Chim. Fr.* **13,** 505 (1988).
35. Chuang, T. A., Brundle, C. R., and Rice, D. W., *Surf. Sci.* **59,** 413 (1976).
36. Marchi, A. J., Di Cósimo, J. I., and Apesteguía, C. R., *in* "Actas XI Simp. Iberoam. Catalysis" (F. Cossio, O. Bermúdez, G. del Angel, and R. Gómez, Eds.), Vol. I, p. 25. IMP, Mexico D. F., 1988.

37. Marchi, A. J., Di Cósimo, J. I., and Apesteguía, C. R., *in* "Proceedings, 9th International Congress on Catalysis" (M. J. Phillips and M. Ternan, Eds.), Vol. II, p. 529. Chem. Institute of Canada, Ottawa, 1988.
38. Bracconi, P., and Dufour, L. C., *CR Acad. Sci. Paris, Ser. C* **270,** 1946 (1970).
39. Boldyrev, V. V., Bulens, M., and Delmon, B., "The Control of Reactivity of Solids" Studies in Surface Science and Catalysis. Elsevier, Amsterdam, 1979.
40. Storch, H., Golumbic, N., and Anderson, R. A., "The Fischer–Tropsch and Related Synthesis" Wiley, New York, 1951.
41. Pouchot, M. T., Verheven, W., and Delmon, B., *Bull. Soc. Chim. Fr.,* 911 (1966).
42. Kawasaki, E., Sanscrainte, J., and Walsh, T. J., *AIChE J.* **8,** 48 (1968).
43. Delmon, B., "Introduction à la Cinetique Hetérogène." Technip, Paris, 1969.
44. Clausen, B. S., Lengeler, B., and Rasmussen, B. S., *Phys. Chem.* **89,** 2319 (1985).
45. Flory, P. J., *J. Am. Chem. Soc.* **58,** 1877 (1936).
46. Biloen, P., and Sachtler, W. M. H., *in* "Advances in Catalysis" (D. D. Eley, H. Pines, and P. B. Weisz, Eds.), Vol. 30, p. 165. Academic Press, New York, 1980.
47. Dry, M. E., *in* "Catalysis-Science and Technology" (J. R. Anderson and M. Boudart, Eds.), Vol. 1, p. 159. Springer-Verlag, Berlin, 1981.
48. Rofer-De Poorter, C., *Chem. Rev.* **81,** 447 (1981).
49. Chinchen, G. C., and Waugh, K. C., *J. Catal.* **97,** 280 (1986).
50. Gusi, S. Trifirò, F., and Vaccari, A., *React. Solids* **2,** 59 (1986).
51. Roberts, D. L., and Griffin, G. L., *J. Catal.* **110,** 117 (1988).
52. Pan, W. X., Cao, R., Roberts, L., and Griffin, G. L., *J. Catal.* **114,** 440 (1988).
53. Chinchen, G. C., Mansfield, K., and Spencer, M. S., *Chemtech* **20,** 692 (1990).
54. Escard, J., Mantin, I., and Sibut-Pinote, R., *Bull. Soc. Chim. Fr.,* 3403 (1970).
55. Sorbelli, A., Trifirò, F., and Vaccari, A., *in* "Proceedings IXth Intern. Symposium on Alcohol Fuels," Vol. 1, p. 61. ECOFUEL, Milano, 1991.
56. Aitchison, L., and Barclay, W. R., *in* "Engineering of non-ferrous metals," Chap. VII. Frowde and Hodder & Stoughton, London, 1923.
57. Van Herwijnen, T., and De Jong, W. A., *J. Catal.* **34,** 209 (1974).